Available online at www.sciencedirect.com
ScienceDirect
Geochimica et Cosmochimica Acta 74 (2010) 1620–1635
Geochimica et Cosmochimica Acta
www.elsevier.com/locate/gca

Combined U–Th/He and $^{40}Ar/^{39}Ar$ geochronology of post-shield lavas from the Mauna Kea and Kohala volcanoes, Hawaii

S.M. Aciego [a,b,*], F. Jourdan [c,d], D.J. DePaolo [b], B.M. Kennedy [b], P.R. Renne [d], K.W.W. Sims [e,f]

[a] Institute for Isotope Geochemistry and Mineral Resources, ETH-Zurich, Clausiusstrasse 25, NW C83.1, Zurich 8092, Switzerland
[b] Center for Isotope Geochemistry, Lawrence Berkeley National Laboratory, Berkeley, CA, USA
[c] Western Australian Argon Isotope Facility, Department of Applied Geology & JdL Center, Curtin University of Technology, GPO Box U1987, Perth, WA 6845, USA
[d] Berkeley Geochronology Center, 2455 Ridge Road, Berkeley, CA 94709, USA
[e] Dept. of Geology and Geophysics, Woods Hole Oceanographic Institute, Woods Hole, MA 02543, USA
[f] Dept. of Geology and Geophysics, University of Wyoming, Laramie, WY 82071, USA

Received 8 January 2009; accepted in revised form 3 November 2009; available online 20 November 2009

Abstract

Late Quaternary, post-shield lavas from the Mauna Kea and Kohala volcanoes on the Big Island of Hawaii have been dated using the $^{40}Ar/^{39}Ar$ and U–Th/He methods. The objective of the study is to compare the recently demonstrated U–Th/He age method, which uses basaltic olivine phenocrysts, with $^{40}Ar/^{39}Ar$ ages measured on groundmass from the same samples. As a corollary, the age data also increase the precision of the chronology of volcanism on the Big Island. For the U–Th/He ages, U, Th and He concentrations and isotopes were measured to account for U-series disequilibrium and initial He. Single analyses U–Th/He ages for Hamakua lavas from Mauna Kea are 87 ± 40 to 119 ± 23 ka (2σ uncertainties), which are in general equal to or younger than $^{40}Ar/^{39}Ar$ ages. Basalt from the Polulu sequence on Kohala gives a U–Th/He age of 354 ± 54 ka and a $^{40}Ar/^{39}Ar$ age of 450 ± 40 ka. All of the U–Th/He ages, and all but one spurious $^{40}Ar/^{39}Ar$ ages conform to the previously proposed stratigraphy and published ^{14}C and K–Ar ages. The ages also compare favorably to U–Th whole rock–olivine ages calculated from ^{238}U–^{230}Th disequilibria. The U–Th/He and $^{40}Ar/^{39}Ar$ results agree best where there is a relatively large amount of radiogenic ^{40}Ar (>10%), and where the $^{40}Ar/^{36}Ar$ intercept calculated from the Ar isochron diagram is close to the atmospheric value. In two cases, it is not clear why U–Th/He and $^{40}Ar/^{39}Ar$ ages do not agree within uncertainty. U–Th/He and $^{40}Ar/^{39}Ar$ results diverge the most on a low-K transitional tholeiitic basalt with abundant olivine. For the most alkalic basalts with negligible olivine phenocrysts, U–Th/He ages were unattainable while $^{40}Ar/^{39}Ar$ results provide good precision even on ages as low as 19 ± 4 ka. Hence, the strengths and weaknesses of the U–Th/He and $^{40}Ar/^{39}Ar$ methods are complimentary for basalts with ages of order 100–500 ka.

1. INTRODUCTION

Hawaiian lavas are used extensively to probe the chemical composition of the Hawaiian mantle plume (Feigenson et al., 1983; West et al., 1988; Frey et al., 1990, 1991; Dixon et al., 1997). Multiple chemical components (Hart et al., 1992; Roden et al., 1994), radial (DePaolo et al., 2001) and asymmetric (Abouchami et al., 2005) zonation of the mantle plume source have been invoked to explain the chemical heterogeneity found in the volcanoes. The ability to characterize the temporal evolution of the volcanoes, and to tie the lava geochemistry to the structure of the mantle plume, is critically dependent on accurate dating of the lavas. Dating has proven to be challenging when using $^{40}Ar/^{39}Ar$ technique, because they are young (<750 ka)

* Corresponding author. Address: Institute for Isotope Geochemistry and Mineral Resources, ETH-Zurich, Clausiusstrasse 25, NW C83.1, Zurich 8092, Switzerland. Tel.: +41 786684269.
E-mail address: aciego@erdw.ethz.ch (S.M. Aciego).

0016-7037/$ - see front matter © 2009 Elsevier Ltd. All rights reserved.
doi:10.1016/j.gca.2009.11.020

and have low concentrations of potassium (Cousens et al., 2003; Sharp and Renne, 2005). In this study U–Th/He measurements of phenocrystic olivine (Aciego et al., 2007) and $^{40}Ar/^{39}Ar$ measurements of groundmass (e.g., Sharp and Renne, 2005) are applied to Late Quaternary lava flows from Hawaii to further test the U–Th/He method on basalts and to improve the detailed geochronology of the youngest volcanoes. This work is in conjunction with a larger study of the trace element and isotopic compositions of the post-shield stage lavas of the Big Island, including samples from Hualalai (Hanano et al., in press). Detailed geochronology is required in order to accurately compare

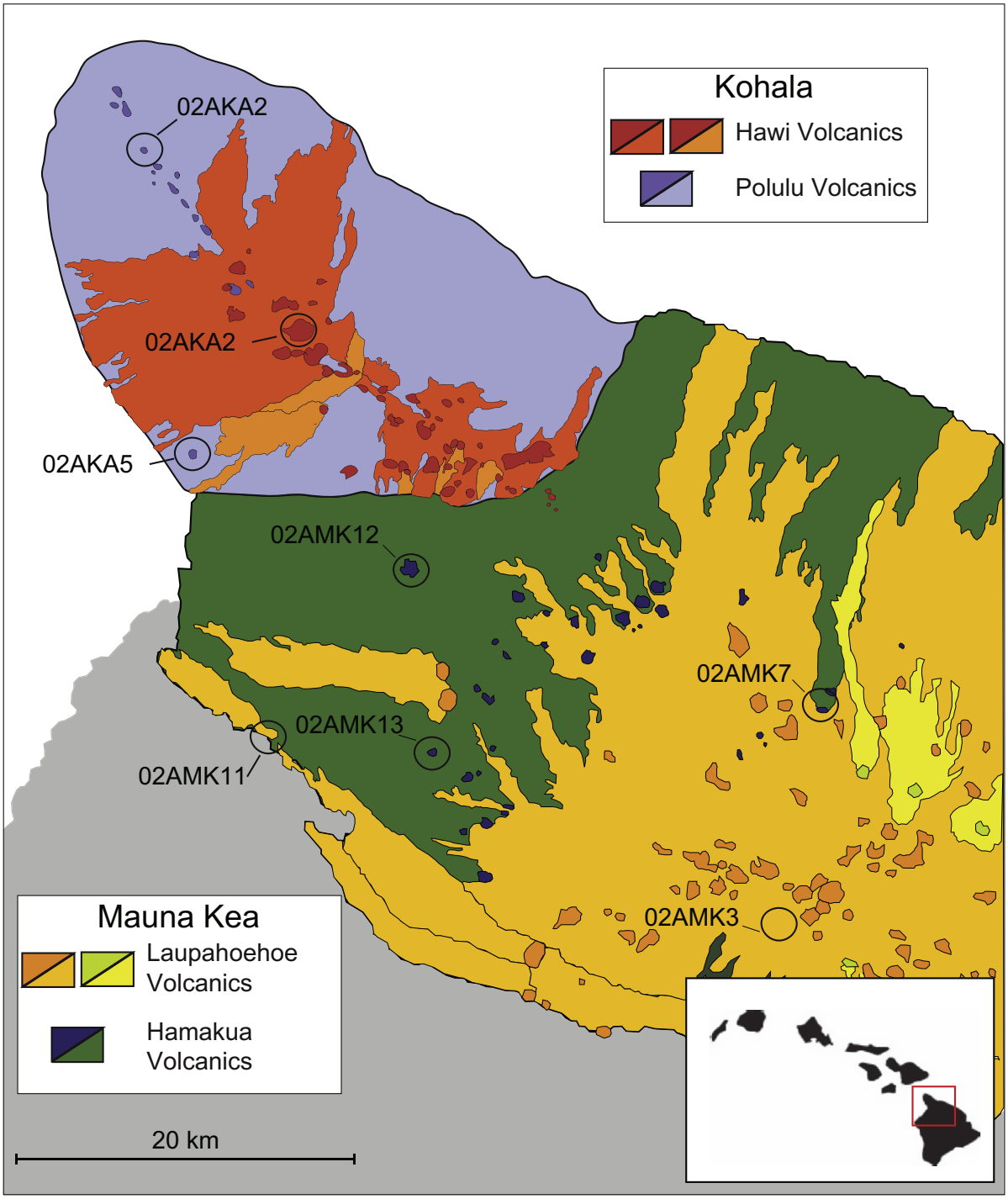

Fig. 1. General geologic map of the Kohala and Mauna Kea volcanoes on the Big Island of Hawaii, inset indicates location relative to the chain of Hawaiian Islands. Most samples were collected from lavas that could be traced back to a specific vent; those vents are noted on the map.

temporal compositional variations of historical lavas from Hualalai with those from the Mauna Kea and Kohala volcanoes.

Hawaiian lavas are challenging targets for the U–Th/He method because they typically have a large component of trapped helium and low concentrations of uranium and thorium. For this study, we focus on transitional tholeiitic to alkalic lavas, which are largely degassed, and have higher K contents, theoretically allowing high precision $^{40}Ar/^{39}Ar$ measurements. Future work will test the U–Th/He method on shield stage tholeiitic basalts, which are traditionally more difficult to date using $^{40}Ar/^{39}Ar$ and may have lower U and Th concentrations, but are older and have abundant olivine.

We present data on post-shield lavas from the older Kohala and younger Mauna Kea volcanoes, which constitute the northwest section of the Island of Hawaii (Fig. 1). On the Kohala volcano, the northern-most on the island, the volcanic units are classified into two groups: the Polulu Volcanic member, containing the transitional tholeiitic to alkali basalts, and the overlying Hawi Volcanic member, the evolved alkalic cap lavas which range in composition from hawaiitic to trachytic. The Kohala volcano entered the post-shield alkalic stage at about 400–500 ka (Wolf et al., 1997). On the Mauna Kea volcano, the lower, transitional basalts are grouped into the Hamakua Volcanic member and the upper, evolved alkalic cap lavas are named the Laupahoehoe Volcanic member (Stearns and Macdonald, 1946). Mauna Kea entered the post-shield alkalic stage at about 100 ka (Wolf et al., 1997). For this work, we sampled both sequences of basalts, but found only the Polulu and Hamakua basalts had high enough abundance of phenocrystic olivine for U–Th/He work.

2. METHODS

2.1. Sample collection and descriptions

Samples were collected from lava flows on the flanks of the Mauna Kea and Kohala volcanoes (Fig. 1), exact locations and elevations are summarized in Table 1. The collection points were road and gulch cuts, where the samples could be collected from more than one meter below the original flow surface to minimize cosmogenic ^{3}He and ^{4}He production, and more than 1 m above the base of the flow which should minimize quenching effects (e.g., glassy groundmass) on the $^{40}Ar/^{39}Ar$ ages. At the collection points, sampled lava flows had no direct overlying units and were less than 50 m thick. The samples are fresh with some occasional minor alteration of the groundmass and, where present, the olivine is unweathered and free of oxidation. The olivine grains have abundant melt inclusions of glass mixed with microcrystalline plagioclase (Fig. 2) as well as minor inclusions of Fe–Ti-oxides and phosphates (likely apatite or fluoroapatite). Major element compositions were measured by XRF on a Philips PW2400 spectrometer at UC Berkeley and the results are summarized in Table 1.

The samples of Hamakua lava from Mauna Kea have abundant olivine and pyroxene phenocrysts, and varying plagioclase phenocryst contents. Microprobe analyses indicate olivine compositions in the range Fo_{75}–Fo_{82} with no zonation in composition across grains. Olivine observed in thin sections show a lack of textural indicators of xenocrystic populations such as resorption rims or sieve cores. In general, all of the samples from Mauna Kea have transitional chemical compositions (Table 1), with more alkalic compositions corresponding to lower olivine abundance.

Table 1
Description of samples.

Sample	Mauna Kea					Kohala		
	AMK3	AMK7	AMK11	AMK12	AMK13	AKA2	AKA5	AKA7
Location								
Latitude	19.77272	19.94378	19.94015	20.00908	19.90715	20.11615	20.04913	20.20917
Longitude	155.47212	155.47448	155.83792	155.81372	155.7051	155.78838	155.83075	155.83312
Altitude (ft)	9990	5312	259	362	2790	3052	442	1559
Shielding (slope; az; inclin. (°))		85; 180; 56						
Description	Massive <1% ol, cpx Microphen	Vesicular 5% ol, cpx 1–5 mm	Massive <1% ol Microphen	Vesicular 5% ol, cpx 1–10 mm	Vesicular 5% ol, cpx 1–5 mm	Massive <1% ol microphen	Vesicular >1% ol 1 mm	Massive <2% ol Microphen
Major elements (wt.%)								
SiO_2	47.96	46.54	49.66	46.72	47.15	50.69	46.90	48.42
TiO_2	3.30	3.79	2.60	1.82	2.96	2.18	3.17	3.32
Al_2O_3	14.17	13.80	16.76	10.09	15.11	16.67	13.06	14.04
Fe_2O_3*	14.54	14.43	11.52	11.84	13.55	10.92	13.31	13.34
MnO	0.19	0.19	0.21	0.16	0.18	0.23	0.18	0.17
MgO	5.74	5.88	4.27	15.95	5.80	3.55	7.75	4.78
CaO	10.77	9.61	6.98	11.19	11.46	6.10	10.65	9.85
Na_2O	2.94	3.39	4.86	1.80	2.76	5.38	2.78	3.15
K_2O	0.80	1.27	1.85	0.44	0.75	1.99	0.80	0.85
P_2O_5	0.41	0.64	0.81	0.20	0.36	1.60	0.49	0.50
Total	100.83	99.54	100.11	100.22	100.08	99.31	99.10	98.41

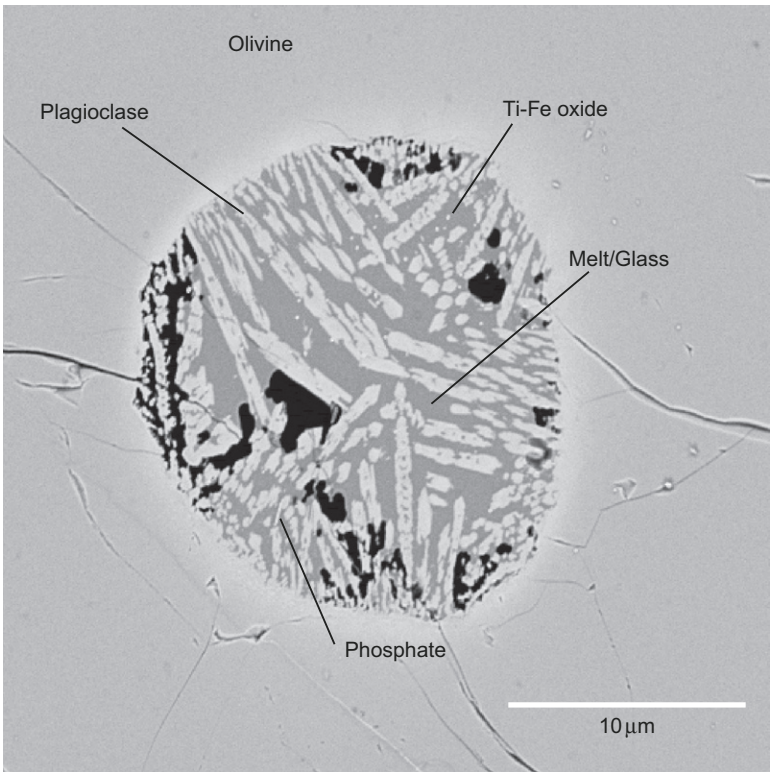

Fig. 2. Electron microprobe backscatter image of micro-inclusion within sample AMK12 showing plagioclase crystallization in contact with the surrounding olivine grain. Also present: glass, Ti–Fe oxides and phosphates.

Sample AMK7 is from a flow originating near the summit, where glacial moraines provide additional stratigraphic context. The samples from Kohala are all alkalic basalt and only one sample contained olivine phenocrysts (AKA5, Fo_{73}). The ages of the flows overlying sample AKA5 have been measured multiple times using K/Ar analyses; the measured ages range from 135 to 149 ka (McDougall, 1969). Fig. 3 shows the stratigraphic relationship between the collected samples and the nearest age markers.

2.2. Sample preparation and analysis

2.2.1. U–Th/He

Rock samples containing olivine were crushed to pea size, a split taken for whole rock powdering, and the remainder sieved, and re-crushed. Olivine grains in the size range 850–1000 μm were magnetically separated and hand-picked. After picking, the olivine separates, approximately 1 g of material, were air abraded to remove the effects of alpha implantation from the decay of groundmass uranium on the helium concentration or alpha ejection loss from the phenocrysts (Min et al., 2006; Aciego et al., 2007; Blackburn et al., 2007). Several attempts were made to separate enough microphenocrysts from samples AMK3, AMK11, AKA2, and AKA7, but the amount of material was not sufficient for helium and U–Th/He analysis. In order to remove enough material by abrasion for microphenocrysts on the order of 100 μm in diameter, more than 70% of the mass must be removed, thereby requiring more than 2 g of olivine grains to start, an amount unattainable with the 5 kg sample sizes collected.

After abrading, the olivine grains were cleaned, air dried, and loaded into a magnetic mortar and pestle for crushing. The crushing in vacuo releases the trapped (initial) helium component leaving the radiogenic and cosmogenic components. Release of the trapped component was optimized to minimize the effects of overcrushing or undercrushing the samples. Overcrushing can result in the release of radiogenic ^{4}He (e.g., Hilton et al., 1999) while undercrushing can result in trapped ^{4}He remaining, between 0.2% and 10% (e.g., Kurz et al., 1996; Williams et al., 2005). Moreira and Madureira (2005) observed a jump in the extracted *in situ* produced helium between 300 and 550 strokes, similar to the jump between 100 and 500 strokes observed by Yokochi et al. (2005). Therefore, samples were crushed using 300 beats in 5 min to minimize the loss of *in situ* produced helium prior to heating. Samples were then sieved to remove the remaining pieces larger than 100 μm, which may have magmatic helium remaining.

The <100 μm size fraction was loaded into platinum packets; powder weights ranged from 0.37 to 0.82 g. The total possible contribution of U and Th from the Pt foil was less than 24 pg. The Pt foil packets were loaded into a resistance furnace designed for low abundance U–Th/He work. Gas release was measured at three temperatures: a 300 °C extraction step to remove any adsorbed gases, a 1500 °C step to release the cosmogenic ^{3}He and the radiogenic ^{4}He by volume diffusion, and a third 1600 °C step to check that gases

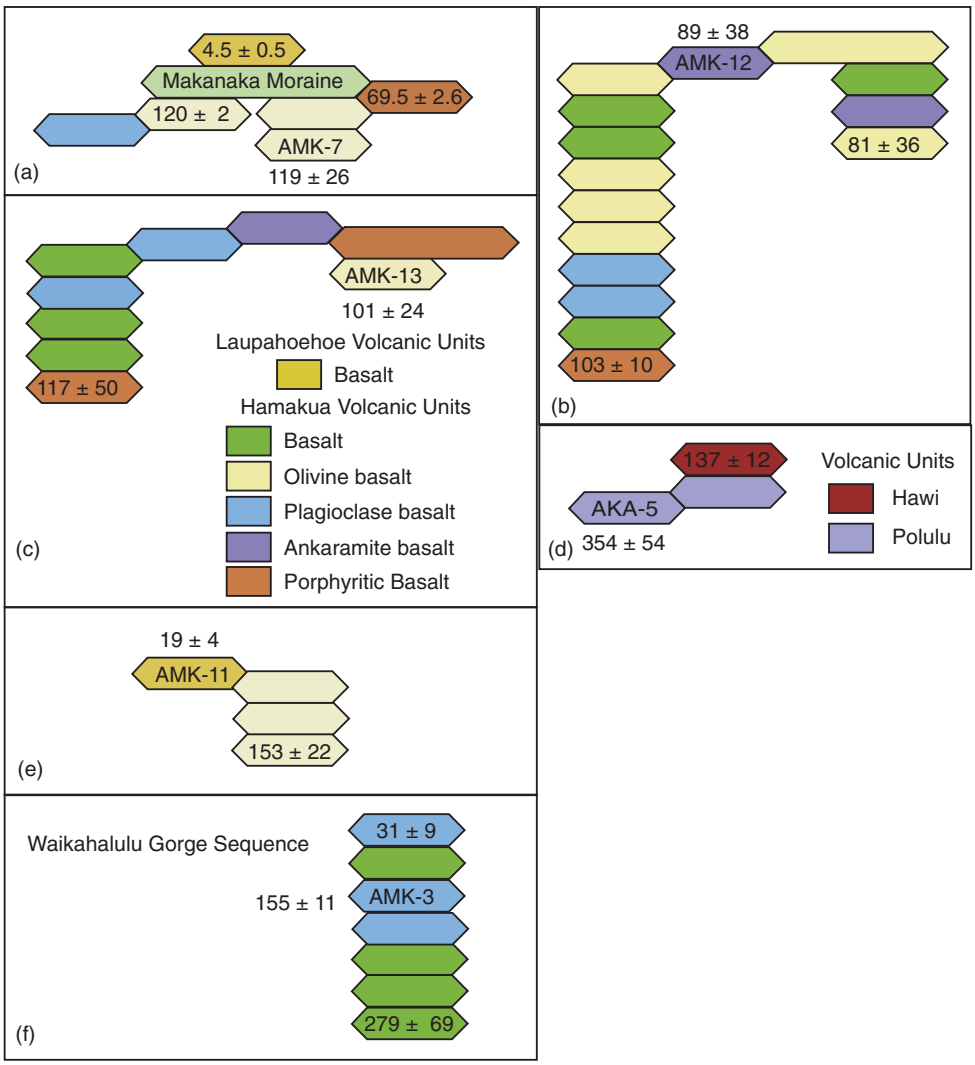

Fig. 3. Simplified stratigraphic columns indicating relationship of samples to nearest age marker and U–Th/He ages. (a) Sample AMK7 constrained by the overlying Makanaka moraine deposited after the last glacial maximum (Porter, 1986), C-14 age of material recovered from Laupahoehoe lavas (Wolf et al., 1997), and overlying lava flow dated by K–Ar (Wolf et al., 1997). (b–d) Samples constrained only by K–Ar ages (McDougall, 1969; Wolf and Morris, 1996; Wolf et al., 1997).

were fully released. Based on olivine diffusivities at 1500 °C (Hart, 1984) for 30 min, total gas extraction should occur in that step and in all cases we found that the gas concentrations released at the 300 and 1600 °C steps were at blank level, therefore numbers reported in Table 2 are the blank subtracted 1500 °C step. Extracted gases were purified on a series of getters and the helium concentrated by absorption on a charcoal trap prior and release directly into the mass spectrometer prior to measurement. Helium abundance and isotopic measurements were conducted on a VG5400 at Lawrence Berkeley National Laboratory equipped with a Faraday cup and an electron multiplier operating in pulse counting mode. Abundance measurements were calibrated using an aliquot of air and a reference sample of helium of known isotopic composition: $R = 2.4$ Ra where Ra is the helium isotopic composition of air ($^3He/^4He = 1.39 \times 10^{-6}$). The detection limit for ^{3}He on the multiplier is 5×10^{-11} nmol; in theory the same detection limit for ^{4}He although the blanks are significantly higher. Blanks were run prior to each sample for both crushing and heating, and varied between 1.3 and 4.0×10^{-6} nmol ^{4}He for the crushers and 1.0 and 3.6×10^{-6} nmol ^{4}He for the furnace, ^{3}He blanks were at the detection limits.

After total gas extraction, the samples packets are retrieved and the fused sample removed from the foil. The samples were dissolved in an HNO_3–HF–$HClO_4$ acid solution. Dissolutions are checked for completeness and formation of any fluorides by centrifuging, and treating dark solids with HNO_3–HF–$HClO_4$ again, white solids (fluorides) with an HCl–Boric acid solution. Aliquots of the solutions were spiked with ^{229}Th and ^{233}U; unspiked aliquots were analyzed for $^{234}U/^{238}U$ and $^{230}Th/^{232}Th$. Isolation of U and Th was accomplished using Tru-Spec® column resin following established procedures (Luo et al., 1997). U and Th isotopic and concentration measurements were made at the Woods Hole Oceanographic Institution. U and Th concentration analyses

were done by isotope dilution on a ThermoFinnegan Element 2 ICP-MS operating in pulse counting mode. Samples were introduced to the mass spectrometer via a CETAC Aridus desolvator. Background counts were evaluated by peak scanning between masses 227 and 240. Standard NBS960 was measured in between every sample to correct for mass fractionation using the natural $^{238}U/^{235}U$ ratio. Samples were measured in triplicate, and the uncertainty in the concentrations, 0.75–1%, reflects the external reproducibility of the repeat measurements. U and Th isotopic compositions were measured on a ThermoFinnegan Neptune MC-ICP-MS. Thorium and uranium isotopic compositions were measured statically with ^{232}Th, ^{238}U, and ^{235}U in Faraday cups and ^{230}Th and ^{234}U in the SEM. Thorium measurements were made with the RPQ filter on, resulting in 85% transmission, abundance sensitivity of 50 ppb over 2 amu, and tail corrections of ^{232}Th on ^{230}Th of ~0.3%. Sample measurements were bracketed with measurements of UCSC ThA, which was used to correct for mass bias and SEM/Faraday gain of the $^{232}Th/^{230}Th$. Sample measurements for uranium were corrected for mass bias using an internal normalization, the natural $^{238}U/^{235}U$ ratio, and bracketed with NBS U10 measurements to determine SEM/Faraday gain. WHOI's analytical protocols for measuring U and Th isotopes and concentrations are detailed in Ball et al. (2008) and Sims et al. (2008a). Accuracy of the spike compositions, and thereby the concentration measurements, and isotopic measurements were monitored by the measurement of rock standard TML, which is well known to have an $[^{230}Th/^{238}U]$ activity ratio of one (e.g., Sims et al., 2008a). The TML powders dissolved and spiked at the same time as the olivine samples had a $[^{230}Th/^{238}U]$ activity ratio of 1.01, which is within the analytical uncertainties of the measurements. Uranium isotopic compositions for all samples were found to be within error of equilibrium, $^{234}U/^{238}U$ activity ratios were 1 ± 0.01. The analytical techniques used for U–Th/He dating are identical to those found in Aciego et al. (2007).

2.2.2. $^{40}Ar/^{39}Ar$

Lava rock chunks were crushed into fine chips. Phenocrysts were removed using conventional Frantz magnetic separation. Groundmass grains (300–500 microns) that showed no sign of alteration were further handpicked and leached in diluted (2N) HF for 1 min and then thoroughly rinsed with distilled water in an ultrasonic cleaner. One irradiation of 15 min duration was performed in the Cd-shielded (to minimize undesirable nuclear interference reactions) CLICIT facility of the TRIGA reactor at Oregon State University. Samples were irradiated in aluminum discs along with the Alder Creek sanidine standard, for which an age of 1.193 Ma is adopted (Nomade et al., 2005). $^{40}Ar/^{39}Ar$ analyses were performed at the Berkeley Geochronology Center using a CO_2 laser. The gas was purified in a stainless steel extraction line using two C-50 getters and a cryogenic condensation trap. Ar isotopes were measured in static mode using a MAP 215-50 mass spectrometer with a Balzers electron multiplier mostly using 10 cycles of peak-hopping. A more complete description of the mass spectrometer and extraction line is given in Renne et al. (1998). Blank measurements were generally obtained before and after every three sample runs. The correction factors for interfering isotopes correspond to the weighted mean of 10 years of measurements of K–Fe and $CaSi_2$ glasses and CaF_2 fluorite in the OSTR reactor: $(^{39}Ar/^{37}Ar)_{Ca} = (7.60 \pm 0.09) \times 10^{-4}$; $(^{36}Ar/^{37}Ar)_{Ca} = (2.70 \pm 0.02) \times 10^{-4}$; and $(^{40}Ar/^{39}Ar)_{K} = (7.30 \pm 0.90) \times 10^{-4}$. Ages were calculated using the decay constants of Steiger and Jager (1977). *J*- and mass discrimination values range from 0.0000680 ± 0.0000003 (0.43%) to 0.0000701 ± 0.0000001 (0.19%) and from 1.00634 ± 0.00216 to 1.00682 ± 0.00242 per dalton (atomic mass unit), respectively. Our criteria for the determination of age plateaus are: (1) to include at least 70% of ^{39}Ar; and (2) to be distributed over a minimum of 3 consecutive steps agreeing at 95% confidence level and satisfying a probability of fit of at least 0.05. Plateau ages are given at the 2σ level and are calculated using the mean of all the plateau steps, each weighted by the inverse variance of their individual analytical error, and assuming that the initial $^{40}Ar/^{36}Ar$ ratio is that of air, 295.5 by convention (Steiger and Jager, 1977). A more recent determination of atmospheric $^{40}Ar/^{36}Ar$ (Lee et al., 2006) yields indistinguishable ages because this value is also used to determine mass discrimination and the effects almost entirely cancel out. Integrated ages (2σ) are calculated using the total gas released for each Ar isotope. Data were also cast in inverse isochron diagrams, and in cases where the $^{40}Ar/^{36}Ar$ intercept ratio is statistically higher than the atmospheric value, the inverse isochron age is used. Inverse isochrons include the maximum number of consecutive steps with a probability of fit $\geqslant 0.05$. Complete descriptions of the analytical procedure are given in Sharp and Renne (2005) and Nomade et al. (2005). Detailed $^{40}Ar/^{39}Ar$ results are shown in Appendix 1 and summarized in Table 2.

3. RESULTS

3.1. U, Th, and He concentrations and isotopic compositions

The U, Th and He concentrations are compiled in Table 2. The ^{4}He concentrations in olivine are in the range 0.64–4.5×10^{-5} nmol/g; three of the samples have concentrations lower than 1.8×10^{-5} nmol/g. The low concentrations limit the accuracy with which ^{4}He concentration can be measured, and if the U and Th concentrations of these samples are representative of Hawaiian olivine, it means that the lower limit age for which the U–Th/He method can be useful for Hawaiian basalt geochronology is about 50 ka using our measurement techniques. Only one sample (AMK7) had cosmogenic ^{3}He (4.59×10^{-9} nmol/g) after crushing. Gas released during crushing has a helium R/Ra (helium isotopic composition normalized to air) of 7.5, while the gas released in melting has an R/Ra of >150 for sample AMK7. All other samples also had crush-release helium compositions between 6.7 and 12 R/Ra, and corresponding concentrations of ^{3}He released in heating below detection limits.

Hawaiian lavas reported in the literature have a large range of trapped helium concentrations, from 2.2 to 1560×10^{-5} nmol/g (Kurz et al., 2004). Even the lower limit of this range is comparable to the amount of radiogenic

Table 2
U–Th concentrations and $^{230}Th/^{232}Th$ compositions of Hawaiian whole rock powders and olivine separates are noted in ppb and square brackets denote activity ratios. Errors in concentration and isotopic composition based on the external reproducibility of the standard TML run at the same time as the samples. Helium concentrations and isotopic compositions are in nmol and R/Ra, the $^{3}He/^{4}He$ ratio in the sample normalized to air. *D* values are the calculated distribution coefficients based on the measured whole rock–olivine U and Th concentrations, Experimental* *D* values are the experimentally determined values from Beattie (1993).

Sample	Whole rock				Olivine								
	U (ppb)	Th (ppb)	$[^{238}U/^{232}Th]$	$[^{230}Th/^{232}Th]$	U (ppb)	Th (ppb)	$[^{238}U/^{232}Th]$	$[^{230}Th/^{232}Th]$	^{4}He (10^{-5} nmol/g)	^{3}He (10^{-9} nmol/g)	R/Ra	D_U	D_{Th}	WR–OL age ka
Kohala														
02AKA5 *crush*									0.96 ± 0.13	0.16 ± 0.03	11.9			
02AKA5 *melt*	567	1744	0.99	1.00	14	41	1.05	1.04	4.51 ± 0.34	n.d.		0.0229	0.0229	
Mauna Kea														
02AMK7 *crush*									3.76 ± 0.28	0.43 ± 0.04	8.2			
02AMK7 *melt*	858	2973	0.88	0.99	28	19	4.68	3.96	1.81 ± 0.19	4.59 ± 0.04	179.2	0.0303	0.0057	163 ± 9
02AMK12(1) *crush*									1.30 ± 0.30	0.19 ± 0.03	10.4			
02AMK12(1) *melt*	218	692	0.96	0.99	13	31	1.26	1.04	0.89 ± 0.19	n.d.		0.0587	0.0419	20 ± 9
02AMK12(2) *crush*									2.25 ± 0.09	0.34 ± 0.05	8.9			
02AMK12(2) *melt*					24	54	1.33	1.13	1.69 ± 0.32	n.d.		0.1087	0.0730	50 ± 10
02AMK13 *crush*									8.14 ± 0.65	0.76 ± 0.06	6.7			
02AMK13 *melt*	531	1518	1.06	1.06	9	15	1.80	1.51	0.64 ± 0.08	n.d.		0.0168	0.0092	102 ± 11
Experimental*												0.00001	0.00001	

* Uncertainties in whole rock U, Th concentrations and isotopic compositions are 1% (2σ), olivine U, Th concentration and isotopic composition uncertainties are 1.5% (2σ)

helium measured in our samples. The post-shield lavas, however, are apparently more thoroughly degassed, as indicated by the low amounts of helium released in crushing. The crushing step yielded small amounts of helium that we assume that if there was any trapped helium remaining in the sample at the heating stage, it was minor compared to the amount of helium released in heating. In the worst case, and 10% of the gas remained after crushing (e.g., Kurz et al., 1996), all of the samples would in fact have much younger ages, which would make the U–Th/He ages less consistent with the $^{40}Ar/^{39}Ar$ ages. However, if the crushing and sieving procedures done were as adequate as those in Williams et al. (2005), and less than 1% of the trapped component remained than the difference in age would be insignificant.

The olivine U and Th concentrations are compared to those of the whole rocks in Table 1. According to trace element partitioning studies, olivine should contain virtually no U and Th (<0.05 ppb) if it forms in equilibrium with typical basalt liquid (Beattie, 1993). The olivine U and Th concentrations are far higher than expected based on published distribution coefficients; instead of a concentration ratio between olivine and whole rock of ca. 10^{-5}, the measured ratios are about 0.01–0.1. The olivine U and Th concentrations are much more variable than those of the whole rocks, and as shown in the duplicate measurements of AMK12; olivine samples from the same lava flow have variable U and Th concentrations. This variability demonstrates that the U and Th are likely held in inclusions, and therefore it is necessary to measure He concentration and U and Th concentrations on the same olivine fraction. The Th/U ratios of the olivine samples are typically lower than those of the whole rocks. The relatively large differences between olivine Th/U and whole rock Th/U indicates that mineral inclusions rather than melt inclusions play the largest role in determining the U–Th concentrations in olivine. Our observations of oxides, phosphates and plagioclase inclusions within the grains is consistent with this hypothesis; Peate et al. (1996) observed highly variable Th/U ratios in mineral separates of magnetite and plagioclase.

3.2. $^{40}Ar/^{39}Ar$ ages

We obtained two plateau ages and one isochron age from Kohala (190 ± 20 to 450 ± 40 ka) and four plateau ages and one isochron age from Mauna Kea (19 ± 4 to 239 ± 84 ka). Associated MSWD and P range from 0.25 to 0.94 and from 0.51 to 0.99, respectively (Fig. 4a and b and Table 3). Associated errors are reported as 2σ uncertainties within the text.

Sample AMK7 yielded a well-defined plateau age of 123 ± 5 ka. For this sample, the percentage of radiogenic $^{40}Ar^*$ is relatively high (11–17%), The isochron age (116 ± 14 ka) agrees very well with the plateau age and yielded a $^{40}Ar/^{36}Ar$ intercept value of 298 ± 4 indistinguishable from the argon atmospheric ratio. For samples AMK3, AMK11, AMK13, AKA5, and AKA7 the fraction of radiogenic $^{40}Ar^*$ (less than 10%) and their K concentration (i.e., ranging from 0.3% to 1.2%) are significantly lower than for sample AMK7 which limits the age precision, although the estimated initial $^{40}Ar/^{36}Ar$ are within 1% of the air value which lends confidence to the plateau age estimates.

Samples AKA2 and AMK12 yielded plateau ages according to our definition of a plateau, but the $^{40}Ar/^{36}Ar$ intercept values (313 ± 22 and 305 ± 6; 2σ) are higher than the atmospheric value and their age spectra follow a slight saddle-shaped pattern. These features suggest the presence of excess $^{40}Ar^*$. For these samples, we use the isochron age calculation, which should provide a better estimate of the crystallization age (Sharp and Renne, 2005). Additionally, AMK12 exhibits a strong tilde-shaped age spectrum. This additional shape suggests that this sample underwent ^{39}Ar and ^{37}Ar redistribution during the neutron irradiation (Onstott et al., 1995; Jourdan et al., 2007). If this is the case, the plateau and isochron calculation cannot be confidently used to define the age of the sample. Furthermore, the fraction of radiogenic $^{40}Ar^*$ is 6–10% lower and the estimated initial $^{40}Ar/^{36}Ar$ is 6 ± 7% higher than the air value. The low percentage of $^{40}Ar^*$ in comparison to the uncertainty in the initial $^{40}Ar/^{36}Ar$ makes the AMK12 age the least reliable of those obtained.

Most of the samples show increasing age and Ca/K over the last 10–20% of the spectrum, at high temperature. These steps also depart from the isochron mixing lines, arguing for a distinct excess $^{40}Ar^*$ reservoirs included in refractory Ca-rich phases (i.e., interstitial pyroxene). These steps were not included in the plateau and isochron age calculation. Overall, all but one (AMK12) of the $^{40}Ar/^{39}Ar$ ages obtained in this study are in agreement with their inferred stratigraphic ages given by previous K/Ar and ^{14}C dates (Fig. 3). Furthermore, the precision of these new $^{40}Ar/^{39}Ar$ ages far surpasses the precision obtained by K/Ar dating on similar lavas, which have uncertainties of 10–30% as shown in Fig. 3.

3.3. U–Th/He ages

Ages were calculated using the measured U, Th and He concentrations and isotopic compositions coupled with the U–Th/He age equation given in Farley et al. (2002) and Aciego et al. (2003). For samples with U-series out of radioactive equilibrium, a correction factor must be applied to take into account variations from secular equilibrium. For samples older than 20 ka and less than 1 Ma, this departure from equilibrium will be dominated by the Th–U fractionation. Therefore, the correction is based on the estimate of the initial U–Th disequilibrium (initial $^{230}Th/^{238}U$ activity $= D_{230}$) at the time of helium closure. D_{230} can be calculated using either the concentrations of U and Th within the whole rock and olivine separates or by using the $^{230}Th/^{238}U$ of the olivine (see Farley et al. (2002) and Aciego et al. (2007) for discussion). In this case we report the ages calculated directly from the olivine; use of the whole rock–olivine concentrations change the ages by −10% for samples AMK12 and AMK13 and by +10% for sample AMK7. Calculated ages are shown in Table 2 and range from 354 ± 54 to 87 ± 40 ka (2σ uncertainties). In general, relatively small amounts of radiogenic ^4He limit the precision of the calculated ages from ±30 to ±50 ka.

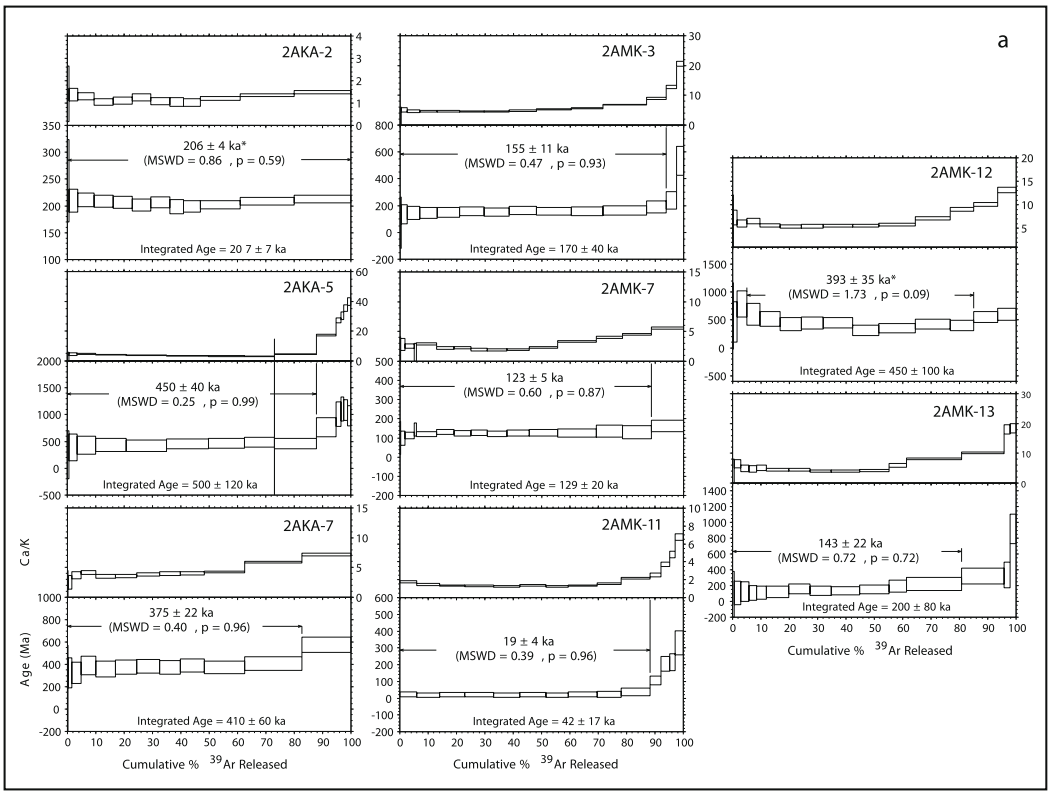

Fig. 4. $^{40}Ar/^{39}Ar$ release patterns. (a) Age spectra: $^{40}Ar/^{39}Ar$ apparent age and related Ca/K ratio spectra of the groundmass separates versus the cumulative percentage of ^{39}Ar released. Errors on plateau (>70% ^{39}Ar released) ages are quoted at 2σ and do not include systematic errors (i.e., uncertainties on the age of the monitor and on the decay constant). MSWD and probability (P) are indicated. Ages in bold represent the most reliable ages for each sample. *age likely containing excess Ar; the isochron calculation technique has been use for these samples. (b) Isochron plots: Inverse isochron plot of $^{36}Ar/^{40}Ar$ versus $^{39}Ar/^{40}Ar$ of two samples having $^{40}Ar/^{36}Ar$ intercept values higher than the atmospheric ratio. Isochron ages are given at 2σ.

Table 3
$^{40}Ar/^{39}Ar$, U–Th/He and ^{3}He ages. Indicates integrated, plateau, isochron $^{40}Ar/^{39}Ar$ ages, U–Th/He crystallization and ^{3}He exposure ages for Kohala and Mauna Kea samples. MSWD for plateau and isochron, percentage of ^{39}Ar degassed used in the plateau calculation, number of analysis included in the isochron, and $^{40}Ar/^{36}Ar$ intercept are indicated. Analytical uncertainties on the ages and $^{40}Ar/^{36}Ar$ intercept are quoted as 2 sigma (2σ). Bold data indicates the accepted $^{40}Ar/^{39}Ar$ ages for a given sample.

Sample	$^{40}Ar/^{39}Ar$ analyses										U–Th–^{4}He–^{3}He analyses	
	Integrated age (ka, ±2σ)	Plateau age (ka, ±2σ)	Total ^{39}Ar released (%)	MSWD	*P*	Isochron age (ka, ±2σ)	*n*	$^{40}Ar/^{36}Ar$ intercept (±2σ)	MSWD	*P*	U–Th/He age (ka, ±2σ)	^{3}He exposure age (ka, ±2σ)
Kohala												
02AKA2	207 ± 7	206 ± 4	100	0.94	0.51	190 ± 20	12	313 ± 22	0.77	0.66		
02AKA5	500 ± 120	450 ± 40	88	0.25	0.99	505 ± 106	11	292 ± 6	0.14	1.00	354 ± 54	–
02AKA7	410± 60	375 ± 22	83	0.40	0.96	460 ± 100	12	289 ± 8	0.20	1.00		
Mauna Kea												
02AMK3	170 ± 40	155 ± 11	94	0.47	0.93	180 ± 60	15	290 ± 8	0.18	1.00		
02AMK7	129 ± 20	**123 ± 5**	89	0.60	0.87	116 ± 14	15	298 ± 4	0.96	0.59	119 ± 26	28 ± 6
02AMK11	42 ± 17	19 ± 4	88	0.39	0.96	n.d.	11	302 ± 16	n.d.	n.d.		
02AMK12(1)	450 ± 100	393 ± 35	76	1.60	0.11	239 ± 84	14	305 ± 6	0.94	0.51	87 ± 40	–
02AMK12(2)											91 ± 36	–
02AMK13	200 ± 80	142 ± 22	81	0.72	0.72	170 ± 60	11	294 ± 6	0.69	0.72	111 ± 24	–

Unlike the $^{40}Ar/^{39}Ar$ ages, there is no additional information (plateau quality, isochron fits, estimate of initial $^{40}Ar/^{39}Ar$) with which to assess the quality of the age determinations. However, for one sample, AMK12, we have duplicate ages of 87 ± 40 and 91 ± 36 ka, which are identical. Unfortunately, that sample has the lowest quality $^{40}Ar/^{39}Ar$ age determination of the samples we measured.

3.4. $^{3}He_C$ age

AMK7 is unique because it was collected from a narrow, shallow gully where it was not possible to collect a sample completely shielded from cosmic radiation exposure. However, although exposed, there was significant cosmic ray shielding due to obstruction of the gully face and the opposite gully wall. We calculated a minimum exposure age of the sample based on the ^{3}He concentration and a production rate. An average equatorial, sea level production rate for ^{3}He in olivine, 103 atoms $g^{-1}\,yr^{-1}$, was scaled for latitude and elevation to 415 atoms $g^{-1}\,yr^{-1}$ (Dunai, 2001) and again to account for 50% azimuthal shielding and a surface dip angle of 90° (Dunne et al., 1999) resulting in a production rate of 101 atoms $g^{-1}\,yr^{-1}$. The calculated age is ~28 ka. This age is not the age of the bottom of the gully, but is an integrated age based on the increasing exposure of the rock as the gully was cut. Given that the production rate of cosmogenic He is negligible more than 10 cm away from the exposed surface, we can infer that the gully was close to 1 m deep at least 28 ka, which is consistent with an eruption age of 120 ka.

4. DISCUSSION

4.1. Comparison of $^{40}Ar/^{39}Ar$, U–Th/He, and U-series ages

As discussed earlier, the Mauna Kea summit lavas have the best age constraints because of the broad glacial moraine coverage. Sample AMK7 must be older than 15 ka, because the Makanaka glacial moraine overlies it. It is also likely to be older than the 100 ka age of the overlying Laupahoehoe Volcanics. The new U–Th/He age of 119 ± 26 ka and $^{40}Ar/^{39}Ar$ plateau age of 123 ± 5 ka confirm this hypothesis. The $^{3}He_C$ age of ~28 ka suggests a slow incision rate that is consistent with the aridity of this region of the Mauna Kea volcano – both the sample collection point and the drainage area for the gully are east of the coastal wet areas on the west coast of the island (Ehlmann et al., 2005). Again, we underscore that for this sample, the $^{40}Ar/^{39}Ar$ age and the U–Th/He age agree well.

For sample AMK12 we have the poorest agreement between the U–Th/He results (89 ± 28 ka) and the $^{40}Ar/^{39}Ar$ result (239 ± 84 ka). As noted above, the Ar results for this sample are not likely to be as reliable as those of the other samples due to the combined effects of low $^{40}Ar^*$ and an uncertain initial $^{40}Ar/^{36}Ar$. While there are both large vertical and lateral stratigraphic distances between the collected samples and the closest previously dated samples, all of the available ages in the region where this sample was collected are between 70 and 150 ka (Wolf et al., 1997). Hence we infer that in this instance the duplicated U–Th/He age may be accurate whereas the $^{40}Ar/^{39}Ar$ age is spuriously old, possibly beyond estimated uncertainty. The fact that this sample is the most tholeiitic in composition (lowest alkalinity, Table 1) highlights the crux of this work: $^{40}Ar/^{39}Ar$ is a powerful dating tool even for young samples, but tholeiites require an alternate dating method, such as U–Th/He.

The minimum age of sample AKA5 from Kohala is constrained by the ~137 ka K–Ar age for a unit (McDougall, 1969) located 200 m stratigraphically higher. The sampled flow is also within the Polulu Volcanic series (Fig. 1), which has a documented age range of 250–500 ka based on several previous K–Ar analyses (McDougall, 1969; McDougall and Swanson, 1972). The calculated U–Th/He age of 354 ± 54

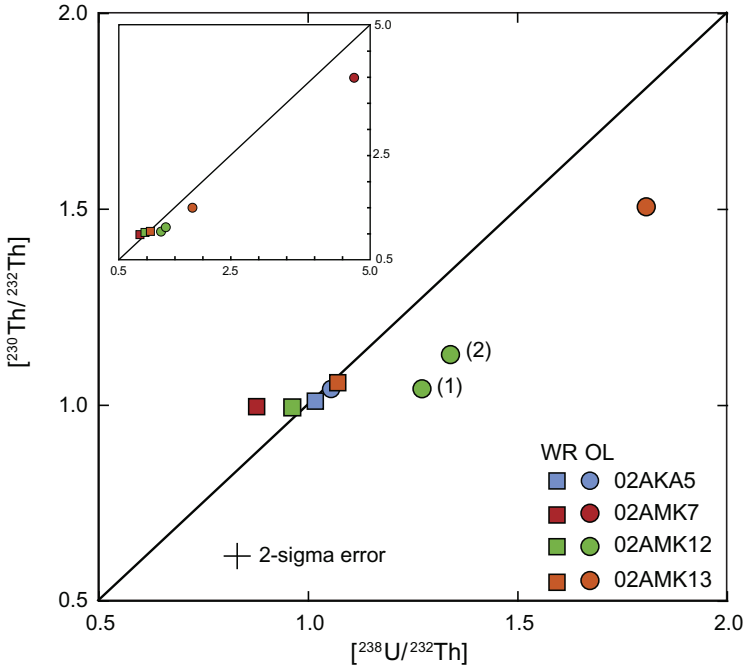

Fig. 5. Activity diagram for the Kohala and Mauna Kea basalts' whole rock powders (WR) and olivine (OL) pairs.

and the $^{40}Ar/^{39}Ar$ age of 450 ± 40 ka, therefore, are both broadly compatible with the previous data although statistically distinguishable.

Our U-series results provide some additional perspective on the reliability of the U–Th/He and $^{40}Ar/^{39}Ar$ ages. The U and Th isotopic composition of the olivine and whole rock samples are plotted on a ^{230}Th–^{238}U activity diagram (Allegre and Condomines, 1976) in Fig. 5. Model 'isochron' ages, with errors based solely on the analytical errors, can be calculated (Table 1) from each whole rock–olivine pair. The calculated isochron age would be the eruption age if the olivine and whole rock had identical initial $^{230}Th/^{232}Th$ and had remained undisturbed since eruption. There are few olivine U–Th isochron data available in the literature with which to compare these results, so we are not certain how well the requirement of identical initial $^{230}Th/^{232}Th$ is likely to be met. One possibility is that the olivine grains did not have an identical initial $^{230}Th/^{232}Th$ to the host lava because they are xenocrystic rather than phenocrystic. Based on the petrographic analysis, this is unlikely, but can not be completely ruled out. In previous work on olivine in basalts (Sims et al., 2007) it was found that internal U-series isochrons that include olivine separates form linear trends, but more accurate and precise age results are generated by removing the olivine from the age calculation, likely because the olivine grains were xenocrystic or antecrystic.

The whole rock and olivine samples from AKA5 both lie on the equiline and have U/Th ratios that differ only slightly. The U–Th data for AKA5 do not define an age, but are consistent with the age being in the 350–450 ka range as determined by the other methods. Sample AMK7 has an OL–WR U–Th age of 163 ± 9 ka, which is somewhat older than our new $^{40}Ar/^{39}Ar$ and U–Th/He ages of ca 120 ka. This difference could be an indication that the olivine in this sample is partly xenocrystic, which could skew the U–Th age to older values but not the U–Th/He age. Sample AMK13 also has a well-defined OL–WR U–Th age of 102 ± 11 ka, which is indistinguishable from the U–Th/He age (111 ± 24 ka) and slightly younger than the $^{40}Ar/^{39}Ar$ (143 ± 22 ka) age. The two olivine analyses from sample AMK12 give two distinct ages of 20 ± 9 ka and 50 ± 10 ka. The older age is closer to the U–Th/He age but much younger than the $^{40}Ar/^{39}Ar$ age for this sample. This may be further evidence that the $^{40}Ar/^{39}Ar$ age for AMK12 is too old.

With the exception of sample AMK7, all of the samples have systematically younger U–Th/He ages than $^{40}Ar/^{39}Ar$ ages. As discussed above, for AMK12, the most likely cause of this discrepancy is $^{40}Ar^*$ excess and/or ^{39}Ar and ^{37}Ar recoil. However, the reason for the age difference is much less clear for the two other samples. AKA5 and AMK13 both yielded $^{40}Ar/^{36}Ar$ intercepts of atmospheric composition on the isochron plot, thereby suggesting that no excess $^{40}Ar^*$ component is present in these samples. There are two possible reasons for the U–Th/He to produce erroneously low ages. The first possibility is diffusive loss, where the higher diffusivity of helium than argon in the crystallized lava flow would result in the observed difference in age. However, as Hart (1984) has shown, olivine in lava flows with thicknesses less than 50 m cool too rapidly for helium loss to occur. Similarly, heat from overlying lavas would dissipate too rapidly for the samples to lose helium, at least at these collection locations where the thicknesses of overlying lavas is 0–10 m. The second possibility is a systematic error in the estimation of U-series disequilibria (Aciego et al., 2007). For the young samples (<300 ka), there is a general agreement (within 10%) between initial $^{230}Th/^{238}U$ (D_{230}) disequilibrium calculated using the

olivine and the initial value calculated using a Th–U fractionation model for crystals and melts (e.g., Farley et al., 2002). Therefore, for these samples we are confident in the errors in the U–Th/He ages due to U-series disequilibria. However, sample AKA5 does have an age that falls in the range of maximum possible error due to uncertainty in D_{230}, between 300 ka and 1 Ma (Farley et al., 2002; Aciego et al., 2007), which could result in uncertainties up to 12%. In this case, using the Th–U fractionation model provides a best estimate for the D_{230}, which lowers the error to 2–5%, well below the difference between the U–Th/He age and the $^{40}Ar/^{39}Ar$ age.

4.2. Implications for future U–Th–He work

A potentially important overall observation is that the U–Th/He ages are consistently either equal to or younger than the $^{40}Ar/^{39}Ar$ (Fig. 6, uncertainties shown are 1σ). The sample with the highest percentage of radiogenic $^{40}Ar^*$ is the one that has the best agreement. While the U–Th/He ages are relatively imprecise, this method may yield accurate results as demonstrated by result on sample AMK7 and these results are encouraging. In any case, as noted above, the uncertainty in the $^{40}Ar/^{39}Ar$ ages may be as high as that for U–Th/He when the samples have low percentages of radiogenic ^{40}Ar. Thus, our results suggest that the U–Th/He chronometer may be a valuable additional tool for dating young mafic volcanic rocks. Substantially more work will be needed, however, before we can be confident about the generality of our conclusions. If the reliability of olivine U–Th/He technique can be demonstrated, we may be able to develop additional insight about which aspects of the Ar data are indicators of unreliable ages by comparing $^{40}Ar/^{39}Ar$ and U–Th/He ages.

This work reinforces the conclusions of Aciego et al. (2007) that U–Th/He dating can be usefully applied to dating basalts in the age range of 50–500 ka, and provides further evidence about the reliability of the U–Th/He method by comparison to the $^{40}Ar/^{39}Ar$ ages on the same samples. The $^{40}Ar/^{39}Ar$ ages determined here also strengthen the possibility of using $^{40}Ar/^{39}Ar$ to precisely measure ages of increasingly younger alkalic basalts, down to the range of radiocarbon dating, although the comparisons with U–Th/He ages suggest that careful attention must be paid to the percentage of radiogenic ^{40}Ar measured and the pattern defined by the age spectrum (i.e., sample AMK12 having 6–10% of $^{40}Ar^*$ and a tilde-shaped age spectrum).

The U–Th/He dating method using olivine of course requires that the samples contain olivine phenocrysts. As noted above and shown by the fewer U–Th/He dates, samples with ~1% microphenocrysts have inadequate olivine for U–Th/He dating. This could be considered a disadvantage in that K–Ar and $^{40}Ar/^{39}Ar$ ages can be determined on groundmass and hence are more widely applicable. On the other hand, volcanic groundmass phases may be more susceptible to cryptic alteration that can affect the age determination. Olivine phenocrysts that are useful for U–Th/He dating are also large enough that alteration can be assessed optically. Even in samples where there is some olivine alteration it may be possible to isolate unaltered olivine. However, the possibility of incomplete separation of the helium reservoirs within the olivine remains an issue that has to be carefully considered. Incomplete release of trapped helium would result in *older* calculated U–Th/He

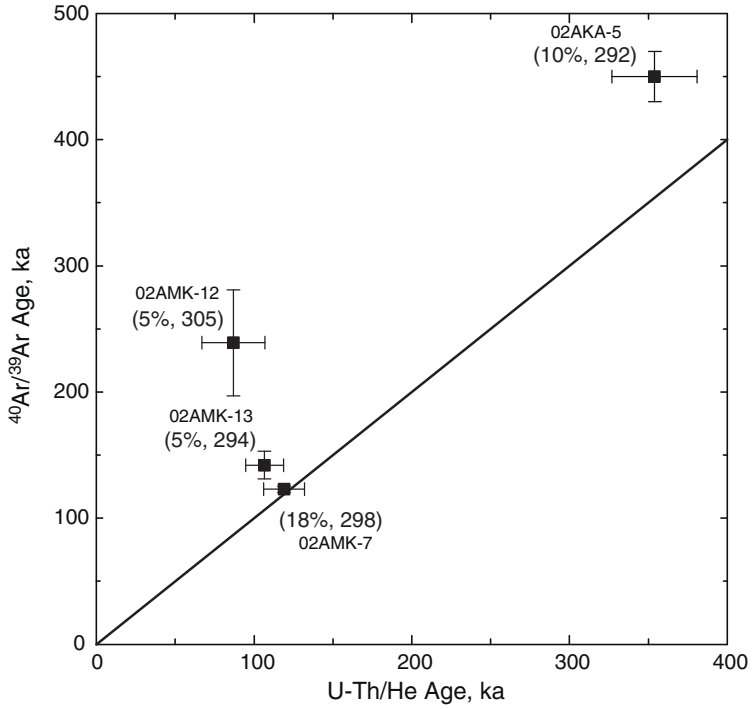

Fig. 6. Comparison of measured $^{40}Ar/^{39}Ar$ ages with U–Th/He ages; $^{40}Ar/^{39}Ar$ ages are plateau ages except for AMK12, which is an isochron age. Error bars are 1σ, and initial Ar composition is noted. Argon plateau ages are older than U–Th/He ages in all samples.

ages. And, while overcrushing could release radiogenic and cosmogenic helium, a significant amount of *in situ* produced helium (>1%) is not likely to be released unless longer crushing times and greater crushing force is used (Moreira and Madureira, 2005). Ultimately, more comparison between U–Th/He and $^{40}Ar/^{39}Ar$ ages are desirable to fully assess the validity of the former technique, and a particularly interesting comparison will be for submarine lavas, where it is well known that there are issues with incomplete degassing of Ar (Dalrymple and Moore, 1968).

A stringent test of the U–Th/He method will come in applying it to a wider range of lava compositions. Other ocean island lavas, (e.g., the Azores, Canary, Comores Islands, Samoa) have similar U and Th concentrations to the alkalic and transitional lavas measured in this work, between 0.6 and 7 ppm U (Chabaux and Allegre, 1994; Sims et al., 1995, 1999, 2008b; Bourdon et al., 1998; Claude-Ivanaj et al., 1998; Claude-Ivanaj et al., 2001; Bourdon et al., 2005; Sims and Hart, 2006). For these lavas, assuming U and Th distribution coefficients of order 0.01, the radiogenic helium production will allow U–Th/He ages to be measured in the same age range as in this work. Other ocean island (e.g., Galapagos, Iceland) and mid-ocean ridge basalts (e.g., EPR) basalts have lower U and Th concentrations, between 0.01 and 0.6 ppm (Hemond et al., 1988; Lundstrom et al., 1999; Sims et al., 2002, 2003; Kokfelt et al., 2003, 2005; Stracke et al. 2003). Therefore, even given optimal analysis conditions of large sample sizes and low blanks, the U–Th/He method will be limited to an older age range, greater than 300 ka. At these low concentrations, the measurement of the $^{230}Th/^{238}U$ disequilibria within the olivine will be especially difficult. However, the measurement may be unnecessary if the Th–U fractionation model is valid. Even older samples (>1 Ma) have the advantage of $^{230}Th/^{238}U$ activity ratios close enough to one for multiple half-lives to make the $^{230}Th/^{238}U$ disequilibria irrelevant in calculating the U–Th/He age (Farley et al., 2002).

One additional complication for future use of the U–Th/He method on OIBs and MORBs is the likely higher initial helium concentration. If samples have both a high initial helium concentration and cosmogenic helium, distinguishing between the radiogenic and initial components of ^{4}He will be difficult, leading to large errors in the age. However, one advantage of submarine samples is that they lack cosmogenic He.

4.3. Implications for Hawaiian plume dynamics

One application of these new ages is to interpret the spatial-temporal evolution of the volcanoes, and in particular, their relationship to the plume source. One way to do this is to map the source of the lava flow, the individual vents, relative to the location of maximum melt supply at the time of eruption (DePaolo et al., 2001). The petrology and geochemistry of the lavas can then provide information about the section of the plume it is sampling: the source material via radiogenic isotopes and melting dynamics via U-series isotopes (see e.g., Sims et al., 1999). However, the combination of geochemical and spatial evidence depends on having reliable ages, which provide the basis for this paleo-mapping. The geochronology of the Big Island has largely been constrained by K–Ar and ^{14}C ages; the sheer number of ages per stratigraphic unit (20–25; Wolf and Morris, 1996) provides a "brute force" basis for the age ranges assigned because the standard deviation of the mean for all of the ages is relatively low (<10%). But, individual K–Ar ages have poor errors – as much as 50%, therefore reconstruction of the vent locations could be in error by as much

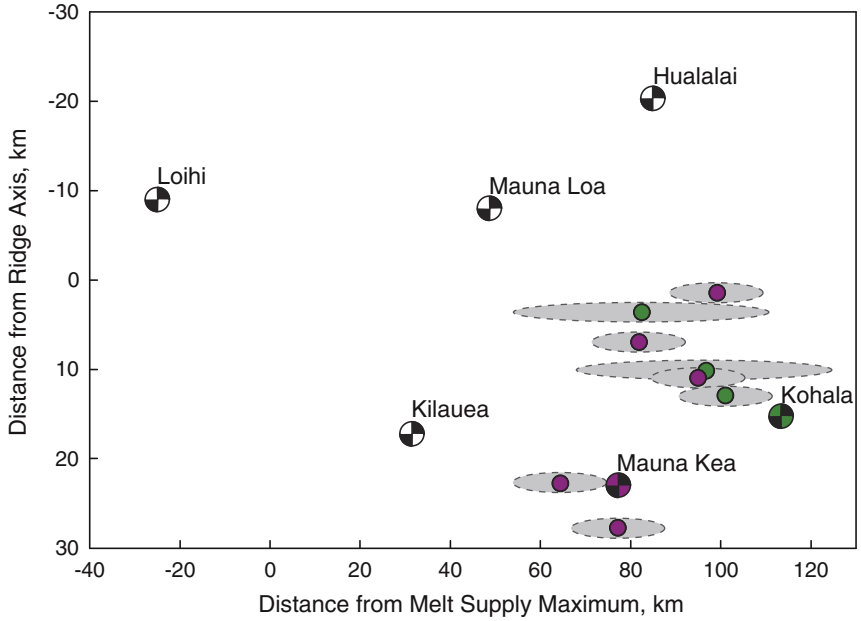

Fig. 7. Reconstructed vent locations of the sampled lavas relative to the Hawaiian plume based on the $^{40}Ar/^{39}Ar$ and U–Th/He ages, and Pacific plate motion of N30W at 9 cm/yr.

as 40 km, the radius of the melting region of the plume. Finer scale analysis of the plume structure and temporal evolution requires more accurate, precise ages, such as those in this work. Fig. 7 illustrates the paleo-mapping for these samples, where the position of the vents relative to the center of the plume, the position of maximum melt supply, is determined based on a Pacific plate motion of N30W at 9 cm/yr. Based on these paleo-locations, the sampled post-shield building lavas of Kohala and Mauna Kea erupted in a front 80–100 km away from the melt supply maximum and 0–15 km away from the center of the plume. Therefore, variations in petrology and geochemistry must be related to magma chamber processes, such as residence time and magma interaction, or temporal variations in the composition of the plume. Both issues which are addressed in Hanano et al. (in press).

5. CONCLUSIONS

The U–Th/He method, applied to olivine phenocrysts in four post-shield basalt lavas from the Mauna Kea and Kohala volcanoes in Hawaii yield ages for lavas in the age range 90–350 ka. The uncertainty in the ages is estimated to be the larger of ±10% or 20 ka at the 1σ level, although duplicate measurements on one lava agree to within a few percent. The age determinations are consistent with previous geologic mapping and geochronological data from the island of Hawaii. Olivine-whole rock U–Th ages measured on the same samples also agree reasonably well with the U–Th/He ages; and the observed discrepancies could have petrological significance. $^{40}Ar/^{39}Ar$ ages measured on groundmass from the same four samples yield identical ages in one case, slightly older ages in two cases, a much older (2×) age in one case. The degree of agreement between the $^{40}Ar/^{39}Ar$ ages and the U–Th/He ages; the best agreement is for the sample with the largest percent radiogenic $^{40}Ar^*$ and identical plateau and isochron ages, the worst agreement is for the tholeiitic sample with a clearly identified perturbed age spectrum, low $^{40}Ar^*$ and higher-than-atmospheric $^{40}Ar/^{39}Ar$ trapped component. For the two intermediate cases, it is not clear yet why we observe some age discrepancy between the two methods and further calibration work is needed. Samples with insufficient olivine for U–Th/He dating yielded robust $^{40}Ar/^{39}Ar$ ages, indicating the advantages of $^{40}Ar/^{39}Ar$ technique for groundmass samples.

The results presented here are encouraging regarding the applicability of U–Th/He geochronology using olivine phenocrysts in sub-aerially-erupted ocean island basalts. The analytical uncertainty in the U–Th/He ages depends on the He content and age of olivine, and limits the usefulness of the method for samples like those measured here to ages that are greater than about 50 ka. The data from this study and that of Aciego et al. (2007) show the method to be useful for lavas in the age range from 50 to 500 ka, and that the U–Th/He ages can complement $^{40}Ar/^{39}Ar$ ages. Further work needs to be done to evaluate other circumstances where the method can complement existing techniques, such as for both subaerial and submarine Quaternary shield stage tholeiitic basalts.

ACKNOWLEDGMENTS

We thank the Hawaiian Homelands division of the State of Hawaii for allowing access to limited areas of the Kohala volcano. This work was supported by the National Science Foundation, EAR0408521, the Ann and Gordon Getty Foundation, and by the Director, Office of Energy Research, Basic Energy Sciences Division of the Department of Energy, under Contract No. De-AC03-76SF00098. T.A. Becker is thanked for analytical assistance in the BGC Ar lab and L. Ball for assistance in the WHOI Plasma Facility. M. Kurz, M. Reid, and an anonymous reviewer are thanked for their helpful comments, which greatly improved the work.

APPENDIX

Ar data summary for the Kohala and Mauna Kea samples. Relative Argon abundances are given in nanoamperes (nA) of amplified beam current. Values are corrected for mass discrimination, blanks, and radioactive decay. Errors in parentheses (1σ) are for the smallest significant digits when not otherwise mentioned. $^{40}Ar^*$, radiogenic argon. Age is based on comparison with the Alder Creek sanidine monitor (1.194 Ma; Nomade et al., 2005) and on the decay constant of Steiger and Jager (1977). *J*- and discrimination values are provided. Laser beam power (W) is provided for step-heated samples. The correction factors for interfering isotopes correspond to the weighted mean of 10 years of measurements of K–Fe and $CaSi_2$ glasses and CaF_2 fluorite in the OSTR reactor: $(^{39}Ar/^{37}Ar)_{Ca} = (7.60 \pm 0.09) \times 10^{-4}$; $(^{36}Ar/^{37}Ar)_{Ca} = (2.70 \pm 0.02) \times 10^{-4}$; and $(^{40}Ar/^{39}Ar)_K = (7.30 \pm 0.90) \times 10^{-4}$.

REFERENCES

Abouchami W., Hofmann A. W., Galer S. J. G., Frey F. A., Eisele J. and Feigenson M. (2005) Lead isotopes reveal bilateral asymmetry and vertical continuity in the Hawaiian mantle plume. *Nature* **434**(7035), 851–856.

Aciego S., Kennedy B. M., DePaolo D. J., Christensen J. N. and Hutcheon I. (2003) U–Th/He age of phenocrystic garnet from the 79 AD eruption of Mt. Vesuvius. *Earth Planet. Sci. Lett.* **216**(1–2), 209–219.

Aciego S. M., DePaolo D. J., Kennedy B. M., Lamb M. P., Sims K. W. W. and Dietrich W. E. (2007) Combining [He-3] cosmogenic dating with U–Th/He eruption ages using olivine in basalt. *Earth Planet. Sci. Lett.* **254**, 288–302.

Allegre C. J. and Condomines M. (1976) Fine chronology of volcanic processes using 238U–230Th systematics. *Earth Planet. Sci. Lett.* **28**, 395–406.

Ball L. A., Sims K. W. W. and Schwieters J. (2008) Measurement of $^{234}U/^{238}U$ and $^{230}Th/^{232}Th$ in volcanic rocks using the Neptune PIMMS. *J. Anal. Atomic Spectrom.* **23**, 173–180. doi:10.1039/b703193a.

Beattie P. (1993) The generation of Uranium series disequilibria by partial melting of spinel peridotite – constraints from partitioning studies. *Earth Planet. Sci. Lett.* **117**(3–4), 379–391.

Blackburn T. J., Stockli D. F. and Walker J. D. (2007) Magnetite (U–Th)/He dating and its application to the geochronology of intermediate to mafic volcanic rocks. *Earth Planet. Sci. Lett.* **259**(3–4), 360–371.

Bourdon B., Joron J. L., Claude-Ivanaj C. and Allegre C. J. (1998) U–Th–Pa–Ra systematics for the Grande Comore volcanics:

melting processes in an upwelling plume. *Earth Planet. Sci. Lett.* **164**, 119–133.

Bourdon B., Turner S. P. and Ribe N. M. (2005) Partial melting and upwelling rates beneath the Azores from a U-series isotope perspective. *Earth Planet. Sci. Lett.* **239**(1–2), 42–56.

Chabaux F. and Allegre C. J. (1994) U-238–Th-230–Ra-226 disequilibria in Volcanics – a new insight into melting conditions. *Earth Planet. Sci. Lett.* **126**(1–3), 61–74.

Claude-Ivanaj C., Bourdon B. and Allegre C. J. (1998) Ra–Th–Sr isotope systematics in Grand Camore Island: a case study of plume–lithosphere interaction. *Earth Planet. Sci. Lett.* **164**, 99–117.

Claude-Ivanaj C., Joron J. L. and Allegre C. J. (2001) 238U–230^{Th}–226Ra fractionation in historical lavas from the Azores: long lived source heterogeneity vs metasomatism fingerprints. *Chem. Geol.* **176**, 295–310.

Cousens B. L., Clague D. A. and Sharp W. D. (2003) Chronology, chemistry, and origin of trachytes from Hualalai volcano, Hawaii. *Geochem. Geophys. Geosyst.* **4**.

Dalrymple G. B. and Moore J. G. (1968) Argon-40: excess in submarine pillow basalts from Kilauea volcano, Hawaii. *Science* **161**(3846), 1132–1135.

DePaolo D. J., Bryce J. G., Dodson A., Shuster D. L. and Kennedy B. M. (2001) Isotopic evolution of Mauna Loa and the chemical structure of the Hawaiian plume. *Geochem. Geophys. Geosyst.* **2**.

Dixon J. E., Clague D. A., Wallace P. and Poreda R. (1997) Volatiles in alkalic basalts from the North Arch volcanic field, Hawaii: extensive degassing of deep submarine-erupted alkalic series lavas. *J. Petrol.* **38**(7), 911–939.

Dunai T. J. (2001) Influence of secular variation of the geomagnetic field on production rates of in situ produced cosmogenic nuclides. *Earth Planet. Sci. Lett.* **193**, 197–212.

Dunne J., Elmore D. and Muzikar P. (1999) Scaling factors for the rates of production of cosmogenic nuclides for geometric shielding and attenuation at depth on sloped surfaces. *Geomorphology* **27**, 3–11.

Ehlmann B. L., Arvidson R. E., Joliff B. L., Johnson S. S., Ebel B., Lovenduski N., Morris J. D., Byers J. A., Snider N. O. and Criss R. E. (2005) Hydrologic and Isotopic Modeling of Alpine Lake Waiau, Mauna Kea, Hawaii. *Pacific Sci.* **59**(1), 1–15.

Farley K. A., Kohn B. P. and Pillans B. (2002) The effects of secular disequilibrium on (U–Th)/He systematics and dating of Quaternary volcanic zircon and apatite. *Earth Planet. Sci. Lett.* **201**(1), 117–125.

Feigenson M. D., Hofmann A. W. and Spera F. J. (1983) Case studies on the origin of basalt. 2. The transition from tholeiitic to alkalic volcanism on Kohala volcano, Hawaii. *Contrib. Mineral. Petrol.* **84**(4), 390–405.

Frey F. A., Wise W. S., Garcia M. O., West H., Kwon S. T. and Kennedy A. (1990) Evolution of Mauna-Kea volcano, Hawaii – petrologic and geochemical constraints on postshield volcanism. *J. Geophys. Res. Solid Earth Planets* **95**(B2), 1271–1300.

Frey F. A., Garcia M. O., Wise W. S., Kennedy A., Gurriet P. and Albarede F. (1991) The evolution of Mauna-Kea volcano, Hawaii – petrogenesis of tholeiitic and alkalic basalts. *J. Geophys. Res. Solid Earth Planets* **96**(B9), 14347–14375.

Hart S. R. (1984) He diffusion in olivine. *Earth Planet. Sci. Lett.* **70**(2), 297–302.

Hart S. R., Hauri E. H., Oschmann L. A. and Whitehead J. A. (1992) Mantle plumes and entrainment – isotopic evidence. *Science* **256**(5056), 517–520.

Hanano D., Weis D., Scoates J. S., Aciego S. M., and DePaolo D.J. (in press) Evidence for ancient depleted components in the Hawaiian mantle plume: Trace element and isotope geochemistry of the Mauna Kea, Kohala and Hualalai volcanoes. *Geochem. Geophys. Geosyst*. doi:10.1029/2009GC002782.

Hemond C., Condomines M., Fourcade S., Allegre C. J., Oskarsson N. and Javoy M. (1988) Thorium, strontium, and oxygen isotopic geochemistry in recent tholeiites in Iceland: crustal influence on mantle-derived magmas. *Earth Planet. Sci. Lett.* **87**, 273–285.

Hilton D. R., Gronvold K., Macpherson C. G. and Castillo P. R. (1999) Extreme He-3/He-4 ratios in northwest iceland: constraining the common component in mantle plumes. *Earth Planet. Sci. Lett.* **173**, 53–60.

Jourdan F., Matzel J. P. and Renne P. R. (2007) 39Ar and 37Ar recoil loss during neutron irradiation of sanidine and plagioclase. *Geochim. Cosmochim. Acta* **71**, 2791–2808.

Kokfelt T. F., Hoernle K. and Hauff F. (2003) Upwelling and melting of the Iceland plume from radial variation of 238U–230Th disequilibria in postglacial volcanic rocks. *Earth Planet. Sci. Lett.* **214**, 167–186.

Kokfelt T. F., Lundstrom C., Hoernle K., Hauff F. and Werner R. (2005) Plume-ridge interaction studied at the Galapagos spreading center: evidence from Ra-226–Th-230–U-238 and Pa-231–U-235 isotopic disequilibria. *Earth Planet. Sci. Lett.* **234**(1–2), 165–187.

Kurz M. D., Kenna T. C., Lassiter J. C. and DePaolo D. J. (1996) Helium isotopic evolution of Mauna Kea volcano: first results from the 1-km drill core. *J. Geophys. Res.* **101**(B5), 11781–11791.

Kurz M. D., Curtice J., Lott D. E. and Solow A. (2004) Rapid helium isotopic variability in Mauna Kea shield lavas from the Hawaiian scientific drilling project. *Geochem. Geophys. Geosyst.* **5**.

Lee J.-Y., Marti K., Severinghaus J. P., Kawamura K., Yoo H.-S., Lee J. B. and Kim J. S. (2006) A redetermination of the isotopic abundances of atmospheric Ar. *Geochim. Cosmochim. Acta* **70**(17), 4507–4512.

Lundstrom C. C., Sampson D. E., Perfit M. R., Gill J. and Williams Q. (1999) Insights into mid-ocean ridge basalt petrogenesis: U-series disequilibria from the Siqueiros transform, Lamont seamounts, and East Pacific Rise. *J. Geophys. Res.* **104**(B6), 13035–13048.

Luo X. Z., Rehkamper M., Lee D. C. and Halliday A. N. (1997) High precision Th-230/Th-232 and U-234/U-238 measurements using energy-filtered ICP magnetic sector multiple collector mass spectrometry. *Int. J. Mass Spectrom. Ion Processes* **171**(1–3), 105–117.

McDougall I. (1969) Potassium–argon ages on lavas of Kohala volcano, Hawaii. *Geol. Soc. Am. Bull.* **80**, 2597–2600.

McDougall I. and Swanson D. A. (1972) Potassium–argon ages of lavas from the Hawi and Pololu volcanic series, Kohala volcano, Hawaii. *Geol. Soc. Am. Bull.* **83**, 3731–3738.

Min K., Reiners P. W., Wolff J. A., Mundil R. and WInters R. L. (2006) (U–Th)/He dating of volcanic phenocrysts with high U–Th inclusions, Jemez volcanic field, New Mexico. *Chem. Geol.* **227**, 223–235.

Moreira M. and Madureira P. (2005) Cosmogenic helium and neon in 11 Myr old ultramafic xenoliths: consequences for mantle signatures in old samples. *Geochem. Geophys. Geosyst.* **6**, 12.

Nomade S., Renne P. R., Vogel N., Sharp W. D., Becker T. A., Jaouni A. B. and Mundil R. (2005) Alder Creek Sanidine (ACs-2): a quaternary 40Ar/39Ar standard tied to the Cobb Mountain geomagnetic event. *Chem. Geol.* **218**, 315–338.

Onstott T. C., Miller M. L., Ewing R. C. and Walsh D. (1995) Recoil refinements; implications for the 40Ar/39Ar dating technique. *Geochim. Cosmochim. Acta* **59**, 1821–1834.

Peate D. W., Chen J. H., Wasserburg G. J., Papanastassiou D. A. and Geissman J. W. (1996) 238U–230Th dating of a geomagnetic excursion in Quaternary basalts of the Albuquerque volcanoes field, New Mexico (USA). *Geophys. Res. Lett.* **23**, 2271–2274.

Porter S. C. (1986) Glaciation of Mauna-Kea, Hawaii. *Quatern. Sci. Rev.* **5**, 181–182.

Renne P. R., Swisher C. C., Deino A. L., Karner D. B., Owens T. L. and DePaolo D. J. (1998) Intercalibration of standards, absolute ages, and uncertainties in Ar-40/Ar-39 dating. *Chem. Geol.* **145**(1–2), 117–152.

Roden M. F., Trull T., Hart S. R. and Frey F. A. (1994) New He, Nd, Pb, and Sr Isotopic constraints on the constitution of the Hawaiian Plume – results from Koolau volcano, Oahu, Hawaii, USA. *Geochim. Cosmochim. Acta* **58**(5), 1431–1440.

Sharp W. D. and Renne P. R. (2005) The Ar-40/Ar-39 dating of core recovered by the Hawaii Scientific Drilling Project (phase 2), Hilo, Hawaii. *Geochem. Geophys. Geosyst.* **6**.

Sims K. W. W., Gill J., Dossetto A., Hoffmann D., Lundstom C. C., Williams R., Ball L. A., Tollstrup D., Turner S. P., Prytulak J., Glessner J., Standish J. J. and Elliott T. (2008a) An inter-laboratory assessment of the Th Isotopic composition of synthetic and rock standards. *Geostand. Anal. Res.* **32**, 65–91.

Sims K. W. W., Hart S. R., Reagan M. K., Blusztajn J., Staudigel H., Sohn R. A., Layne G. D., Ball L. A. and Andrews J. (2008b) ^{238}U–^{230Th}–^{226}Ra–^{210}Pb–^{210}Po,^{232}Th–^{228}Ra and ^{235}U–^{231}Pa constraints on the ages and petrogenesis of Vailulu and Malumalu lavas, Samoa. *Geochem. Geophys. Geosyst.* **9**, Q04003. doi:10.1029/2007GC001651.

Sims K. W. W., Ackert R. P., Ramos F. C., Sohn R. A., Murrell M. T. and DePaolo D. J. (2007) Determining eruption ages and erosion rates of Quaternary basaltic volcanism from combined U-series disequilibria and cosmogenic exposure ages. *Geology* **35**(5), 471–474.

Sims K. W. W. and Hart S. R. (2006) Comparison of Th, Sr, Nd and Pb Isotopes in Oceanic basalts: implications for Mantle heterogeneity and Magma genesis. *Earth Planet. Sci. Lett.* **245**, 743–761. doi:10.1016/j.epsl.2006.02.030.

Sims K. W. W., Blichert-Toft J., Fornari D. J., Perfit M. R., Goldstein S. J., Johnson P., DePaolo D. J. and Michaels P. (2003) Aberrant Youth: chemical and isotopic constraints on the young off-axis lavas of the East Pacific Rise. *Geochem. Geophys. Geosyst.* **4**. doi:10.1029/2002GC000443.

Sims K. W. W., Goldstein S. J., Blichert-Toft J., Perfit M. R., Kelemen P., Fornari D. J., Michael P., Murrell M. T., Hart S. R., DePaolo D. J., Layne G. D. and Jull M. (2002) Chemical and isotopic constraints on the generation and transport of melt beneath the East Pacific Rise. *Geochim. Cosmochim. Acta* **66**, 3481–3504. doi:10.1016/S0016-7037(02)00909-2.

Sims K. W. W., Murrell M. T., DePaolo D. J., Baldridge W. S., Goldstein S. J., Clague D. and Jull M. (1999) Porosity of the melting zone and variations in the solid mantle upwelling rate beneath Hawaii: inferences from ^{238}U–^{230}Th–^{226}Ra and ^{235}U-^{231}Pa disequilibria. *Geochim. Cosmochim. Acta* **63**, 4119–4138. doi:10.1016/S0016-7037(99)00313-0.

Sims K. W. W., DePaolo D. J., Murrell M. T., Baldridge W. S., Goldstein S. J. and Clague D. (1995) Mechanisms of magma generation beneath Hawaii and Mid-Ocean ridges: U–Th and Sm–Nd isotopic evidence. *Science* **267**, 508–512. doi:10.1126/science.267.5197.508.

Stearns H. T. and Macdonald G. A. (1946) Geology and groundwater resources of the Island of Hawaii. In *Hawaii Division of Hydrography Bulletin*, vol. 9, p. 363.

Steiger R. H. and Jager E. (1977) Subcommission on geochronology – convention on use of decay constants in geochronology and cosmochronology. *Earth Planet. Sci. Lett.* **36**(3), 359–362.

Stracke A., Zindler A., Salters V. J. M., McKenzie D. and Gronvold K. (2003) Dynamics of melting beneath Theistareykir, northern Iceland. *Geochem. Geophys. Geosyst.* **4**.

West H. B., Garcia M. O., Frey F. A. and Kennedy A. (1988) Nature and cause of compositional variation among the alkalic cap lavas of Mauna Kea volcano, Hawaii. *Contrib. Mineral. Petrol.* **100**, 383–397.

Williams A. J., Stuart F. M., Day S. J. and Philips W. M. (2005) Using pyroxene microphenocrysts to determine cosmogenic He-3 concentrations in old volcanic rocks: an example of landscape development in central Gran Canaria. *Quatern. Sci. Rev.* **24**, 211–222.

Wolf E. W. and Morris J. D. (1996) Geologic Map of the Island of Hawaii. In *Geologic Investigations Series Ma I-2524-A*. US Geological Survey.

Wolf E. W., Wise W. S. and Dalrymple G. B. (1997) The Geology and Petrology of Mauna Kea Volcano, Hawaii – A Study of Postshield Volcanism. US Geological Survey. pp. 129.

Yokochi R., Marty B., Pik R. and Burnard P. (2005) High $^{3}He/^{4}He$ ratios in peridotite xenoliths from SW Japan revisited: evidence for cosmogenic ^{3}He released by vacuum crushing. *Geochem. Geophys. Geosyst.* **6**.

Associate editor: Bernard Marty